Structure and Fragility of Normal and Invert Lanthanum Borate Glasses: Results from ^{11}B and ^{17}O NMR Spectroscopy and Calorimetry

[1]R.K. Swanson, [2]J.F. Stebbins, [3]T.M. Yeo, [4]Y. Xu, [4]I. Hung, [4]Z. Gan,

[1]S.J. McCormack, [1]S. Sen

[1]Deparment of Materials Science and Engineering, University of California at Davis, Davis, California 95616, USA

[2]Department of Earth and Planetary Sciences, Stanford University, Stanford, California 94305, USA

[3]Graduate Institute of Ferrous & Energy Materials Technology, Pohang University of Science and Technology (POSTECH), Pohang, 37673, Republic of Korea

[4]National High Magnetic Field Laboratory, 1800 East Paul Dirac Drive, Tallahassee, Florida 32310, USA

Abstract

The structure of select normal and invert $(La_2O_3)_x(B_2O_3)_{100-x}$ glasses with $22 \leq x \leq 60$, synthesized using conventional and containerless levitation melt-quenching, is studied using ^{11}B and ^{17}O NMR spectroscopy. The results indicate that the structure of normal glasses with $22 \leq x \leq 30$ is characterized by a borate network of B-O-B bridging oxygen (BO) linkages between BO_3 and BO_4 units and non-bridging oxygen (NBO) with La acting as a charge balancing modifier cation. In contrast, the invert glasses with $55 \leq x \leq 60$ consist of a network of La-O polyhedra connected via La-O-La linkages i.e. "free-oxide" ions and via La-NBO-B linkages with interspersed $[BO_3]^{3-}$ units. This structural evolution in lanthanum borate glasses is consistent with the composition dependence of their glass transition temperature. The temperature dependent boron and oxygen speciation in these glasses are linked to their calorimetrically determined fragility index.

1. Introduction

Typically, oxide glasses are derived from liquids that are melted mixtures of network forming oxides such as SiO_2, P_2O_5 or B_2O_3 and of network modifier oxides that are most commonly one or more of the alkali and alkaline-earth oxides and less often other modifiers such as transition metal and rare earth oxides [1,2]. The melting results in a redistribution of bonds between oxygen and network forming and modifying cations. Such a redistribution yields three fundamentally different types of oxygen environments in the liquid and in the derived glass [3-9]. These are bridging oxygen (BO) that are shared between two Si, B or P atoms, non-bridging oxygen (NBO) that are bonded to only one network-forming cation and to one or more network-modifier cations, and free-oxide ion (FO) that are oxygen atoms only bonded to two or more network-modifier cations. Early thermodynamic studies of oxide liquids, particularly of molten silicate slags, have considered a homogeneous equilibrium between these oxygen species in the liquid that can be written as [5]:

$$FO + BO \rightleftharpoons 2NBO \qquad (1)$$

An apparent equilibrium constant for this reaction, ignoring the activity coefficients, can be written as:

$$K = [NBO]^2 / ([FO] \times [BO]) \qquad (2)$$

The reaction in Eq. 1 is usually strongly exothermic for NBO formation. Thus, addition of network modifiers to SiO_2 or P_2O_5 in the normal glass-formation range produces a mixture of BO and NBO, with FO generally low enough to be undetectable and thus K may be approximated as ∞ for models of major speciation [5]. On the other hand, the appearance of

NBO is delayed in the case of B_2O_3-based glasses/liquids until the modifier oxide concentration exceeds ~30-40 mol% as the initial addition of network modifiers results in an increase in the B-O coordination number from 3 to 4 to accommodate the concomitant increase in the O/B ratio. The appearance of FO becomes inevitable in liquids/glasses with modifier-rich compositions such that the O/(Si,P) ratio exceeds 4 or the O/B ratio exceeds 3 (if all B is three-coordinated). However, it may be noted that small amounts of FO may appear in liquids/glasses with even slightly lower oxygen content than these limiting values, consistent with the entropic stabilization of such species [5]. For example, a number of previous ^{17}O nuclear magnetic resonance (NMR) spectroscopic investigations of a variety of orthosilicate glasses and amorphous thin films with O/Si = 4 have indicated a shift of the equilibrium in Eq. 1 to the left such that K in Eq. 2 decreases from ∞ to values ranging between ~ 1 and ~1000 [5]. The value of K is also expected to decrease with increasing temperature and ionic field strength (valence divided by the square of the nearest-neighbor cation-oxygen distance) of the modifier cation. Recent thermodynamic calculations have indicated that the oxygen speciation reaction in Eq. 1 may have a measurable contribution towards the configurational entropy of the oxide liquid [5]. Thus, following the Adam-Gibbs formalism of shear relaxation, such speciation can contribute significantly to the fragility of the liquid where the fragility index *m* of a liquid is related to the departure of the temperature dependence of its viscosity η from an Arrhenius behavior and it is defined as: $m = \left.\frac{d\log_{10}\eta}{dT_g/T}\right|_{T=T_g}$, with T_g being the glass transition temperature of the liquid [10,11].

Unlike silicates, the nature of oxygen speciation in highly modified phosphates and borates with O/P ≥ 4 or O/B ≥ 3 remains largely unexplored except for a few studies on borates [12-15], primarily due to the extreme difficulty in glass formation in these systems for such

compositions. This difficulty in synthesis has recently been overcome by Masuno and coworkers who used containerless processing to demonstrate glass-formation in RE_2O_3-B_2O_3 (RE = rare earth) binary systems over a wide range of Re_2O_3 concentrations and for a variety of rare earth elements [16,17]. Glasses with up to ~ 55 to 65 mol% RE_2O_3 (O/B going up to 3.3 to 4.3) were synthesized using CO_2 laser melting and aerodynamic levitation where crystallization was avoided by suppressing heterogeneous nucleation and by fast quenching by turning off the laser [17]. These glasses with unusually high RE content were found to be characterized by unique physical attributes such as high refractive index and unusual magnetooptical properties [16,17]. However, these glasses with networks extensively modified via the addition of large concentrations of high field strength RE cations also lend themselves well for studying the oxygen speciation reaction represented by Eq. 1. Here we report the results of such a study of $(La_2O_3)_x$ $(B_2O_3)_{100-x}$ glasses with $55 \leq x \leq 60$, using high-resolution ^{11}B and ^{17}O NMR spectroscopy. We also present results on the temperature dependent speciation of trigonal and tetrahedral B in a $(La_2O_3)_x$ $(B_2O_3)_{100-x}$ glass with composition in the conventional bulk glass-forming region with $x = 25$. The compositional evolution of the fragility index m of $(La_2O_3)_x$ $(B_2O_3)_{100-x}$ glasses is investigated using differential scanning calorimetry (DSC) and its connection to the boron and oxygen speciation in the structure is sought.

2. Experimental

2.1. Glass synthesis and characterization

$(La_2O_3)_x$ $(B_2O_3)_{100-x}$ glasses with $x = 22$ and 25 were synthesized by melting a stoichiometric mixture of the constituent oxides (99.9% La_2O_3 and 99.99% B_2O_3, Alfa Aesar) at 1400 °C for 1 hour in air in a platinum crucible and subsequently quenching by dipping the bottom of the

crucible in water. Two samples of $(La_2O_3)_{25}(B_2O_3)_{75}$ glass with different fictive temperatures T_f were obtained by (i) quenching the melt in water (high T_f) and (ii) by annealing for 30 minutes at the calorimetric T_g followed by shutting down the furnace power (low T_f). These two glasses are designated as "water-quenched" and "furnace-cooled" in the subsequent discussion. On the other hand, $(La_2O_3)_x (B_2O_3)_{100-x}$ glasses with x= 30, 55 and 60 were synthesized using a containerless levitation technique. The glass with x= 30 was synthesized from regular oxide reagents while, glasses with x= 25, 55 and 60 were prepared with ^{17}O isotope enriched B_2O_3. The latter was obtained by dehydration and melting of boric acid (H_3BO_3) enriched to ~ 42% in ^{17}O, which was synthesized by hydrolysis of BCl_3 with $H_2{}^{17}O$ at about 0 °C in $CHCl_3$ solution [18]. For containerless levitation melting the reagents were finely ground with a mortar and pestle and pressed into a single pellet. The pellet was calcined for 12h at 600 °C and crushed again to mix with ~ 18 mass% water, ~ 10 mass% Darvan as dispersant, and ~ 9 mass% cellulose as a binding agent. The green body thus obtained was formed into ~ 10 beads that were subsequently calcined at 1000 °C for 12h. The water, Darvan, and cellulose were vaporized during calcination and therefore do not contribute to the composition of the resulting beads. Each bead was sanded down to ~50% of its original mass to have the acceptable size for the levitator nozzle. The beads were then levitated in oxygen and heated to ~ 2000 °C for ~ 10 s using a 400 W CO_2 laser (10.6 µm; Synrad FSi401SB; Mukilteo, WA). The molten beads were quenched by shutting off the laser. The resulting glass beads ranged in diameter between 1.0 and 1.5 mm. The La_2O_3 content of these beads was determined using electron probe microanalysis (Cameca SX-100) and was found to be within ± 0.45 mol% of the nominal composition. Density of these glasses was measured using a gas expansion pycnometer (Micromeritics AccuPyc II 1340) at

20°C using helium (6N purity) as the displacement gas and was found to be within ±0.5% of the reported values in the literature [16,17].

2.2. Fragility from Calorimetry and viscosity

The dependence of the fictive temperature T_f of select $(La_2O_3)_x(B_2O_3)_{100-x}$ glasses with x= 22, 25, 30, and 55 on the cooling/heating rate were measured using DSC (LABSYS evo STA 1600, Setaram). For each glass composition, approximately 15 to 25 mg of sample was taken in a platinum crucible. The samples were heated at a specific rate of q K/min under a nitrogen atmosphere to 30 K above T_g to erase any thermal history, cooled down to T_g – 50 K and then reheated at the same rate. The T_f is taken as the onset of the endothermic glass transition signal during reheating and was measured as a function of q ranging between 2 and 40 K/min. T_g was taken as the T_f obtained at a heating/cooling rate of q = 10 K/min. The estimated error in T_f is within ± 2 K. The q dependence of T_f for these glasses is shown Fig. 1. The slope of the linear dependence of $1/T_f$ on $ln\ q$ yields the activation energy E_g for enthalpy relaxation. The calorimetric fragility index m can then be obtained from E_g using the relation [19]: $= \frac{E_g}{RT_g \ln 10}$.

The fragility index of the $(La_2O_3)_{25}(B_2O_3)_{75}$ liquid was also estimated from the temperature dependence of its viscosity. The relatively high thermal stability of this composition against crystallization enabled viscosity measurements in the supercooled state over a temperature range ~ 850-1200 °C corresponding to viscosity ranging between ~ $10^{2.5}$ and 0.3 Pa.s. The viscosity was measured on cooling the liquid from 1400 °C in air, using a rotational viscometer (VIS 413, TA Instruments) equipped with a platinum crucible and spindle.

2.3. NMR spectroscopy

The ^{11}B MAS NMR spectra of select $(La_2O_3)_x(B_2O_3)_{100-x}$ glasses with x= 22, 25, 30, and 55 were collected at UC Davis using a Bruker Avance-III spectrometer operating at a resonance frequency of 160.5 MHz (magnetic field 11.7 T) and a 4 mm Bruker CPMAS probe. Samples were taken in ZrO_2 rotors and were spun at a rate of 12 kHz. The ^{11}B MAS NMR spectra were acquired using a solids 15° pulse, a recycle delay of 0.5 s, and 1000 to 5000 transients were averaged and Fourier-transformed to obtain each spectrum. The ^{11}B MAS NMR spectrum of the $(La_2O_3)_{55}(B_2O_3)_{45}$ glass was also collected at the National High Magnetic Field Laboratory (NHMFL) in Tallahassee, Florida using a Bruker Avance NEO spectrometer operating at a resonance frequency of 266.8 MHz (magnetic field 19.6 T) and a 3.2 mm low-E double-resonance probe. Crushed glass sample was taken in a ZrO_2 rotor and spun at a rate of 10 kHz. ^{11}B 1D MAS NMR spectrum was acquired using a rotor-synchronized spin-echo sequence using an interpulse delay of 25 rotor periods for a whole spin-echo signal, with 4.8 μs 90° pulse and 64 transients. The ^{17}O MAS NMR spectrum of the ^{17}O isotope enriched $(La_2O_3)_x(B_2O_3)_{100-x}$ glass with x = 25 was collected at the NHMFL using the ultra-high field (35.2 T) series-connected hybrid magnet (^{17}O resonance frequency 203.4 MHz) using a Bruker Avance NEO console and a 3.2 mm MAS probe designed and constructed at the NHMFL. Crushed glass sample was taken in a ZrO_2 rotor and was spun at 16 kHz. Rotor-synchronized QCPMG (Quadrupolar Carr–Purcell–Meiboom–Gill) sequence was used to acquire multiple echoes for sensitivity enhancement. A total of 24 echoes with 16 rotor periods for each echo were acquired under 16 kHz MAS frequency. A WURST (Wideband-Uniform Rate-Smooth Truncation) pulse with 320 kHz offset and 10 kHz *rf* field was applied to the satellite transitions for enhancing the central transition polarization. The excitation and refocusing pulses for the QCPMG sequence were 3 and 6 μs,

respectively. The strong ^{17}O signal from this glass sample allowed the spectrum to be acquired with a recycle delay of 2s and 1024 transients. Spectra were collected at multiple spinning speeds to determine the location of spinning sidebands.

The ^{17}O MAS NMR spectra of the ^{17}O isotope enriched $(La_2O_3)_x(B_2O_3)_{100-x}$ glasses with x = 55 and 60 were collected at the NHMFL using a Bruker Avance III-HD spectrometer operating at a resonance frequency of 108.5 MHz (magnetic field 18.8 T) and a 3.2 mm low-E triple-resonance probe. Crushed glass samples were taken in an ^{17}O-background free sialon rotor and were spun at 10 kHz. Rotor-synchronized QCPMG sequence was used to acquire multiple echoes for sensitivity enhancement. A total of 24 echoes with 10 rotor periods for each echo were acquired under 10 kHz MAS frequency. A WURST pulse with 300 kHz offset and 17 kHz *rf* field was applied to the satellite transitions for enhancing the central transition polarization. The excitation and refocusing pulses for the QCPMG sequence were 2.5 and 5 μs, respectively. The relatively weak ^{17}O signal from these samples required the spectra to be collected with a recycle delay of 8s and 27220 transients. The ^{17}O chemical shift for all spectra was referenced externally to distilled H_2O at 0 ppm.

3. Results and Discussion

3.1. ^{11}B NMR

The low-field (11.7 T) ^{11}B MAS NMR spectra of select $(La_2O_3)_x(B_2O_3)_{100-x}$ glasses are shown in Fig. 2. These spectra display two distinct resonances. The resonance at high frequency (higher ppm) is characterized by a quadrupolar-broadened line shape that is characteristic of trigonal BO_3 units, while the Gaussian line shape at lower frequency near ~ 0.5 ppm corresponds to the tetrahedral BO_4 units. The areas under these resonances yield the relative fractions of the

BO_3 and BO_4 units in the glass structure. The compositional variation of the relative fraction of BO_4 units thus obtained for the $(La_2O_3)_x(B_2O_3)_{100-x}$ glasses is shown in Fig. 3. The fraction of BO_4 in these glasses appears to go through a maximum near x = 25 (O/B = 2) and becomes undetectable in glasses with $x \geq 55$. These results are in general agreement with those reported for La-borate glasses in previous studies by Masuno and coworkers as well as with the trends observed in borate glasses with low field strength modifier cations such as the alkali borates with similar O/B ratios (Fig. 3) [16,17,20]. However, we note that for comparable compositions the BO_4 fractions reported by Masuno et al. [16] are systematically somewhat lower than those observed in the present study. This difference may possibly result from a difference in the T_f between the two sets of glasses (see below) and/or due to some loss in B_2O_3 due to evaporation during the high-temperature synthesis. We have noticed such preferential loss of B_2O_3 during levitation laser melting as well and have compensated for it accordingly in the starting batch compositions.

The apparent absence of BO_4 units in glasses with $x \geq 55$ as observed in Fig. 2 is consistent with their high O/B ratio, which becomes sufficient to form "isolated" $[BO_3]^{3-}$ units without B-O-B linkages. In fact, Masuno et al. [16] reported the onset of the disappearance of BO_4 units at x = 50, where the oxygen concentration becomes just sufficient (O/B = 3) for the formation of $[BO_3]^{3-}$ units. However, a rather small but significant departure from this expected behavior is observed in the high field (19.6 T) ^{11}B MAS NMR spectrum of the $(La_2O_3)_x(B_2O_3)_{100-x}$ glass with x = 55 (Fig. 2), which displays a weak resonance centered near ~ 2.5 ppm that corresponds to ~ 0.5% of the B atoms being present as BO_4 units in this glass. Such a significant shift of this resonance to higher ppm values was also reported in a recent study on lead borate glasses with O/B = 3.5, where it was ascribed to a shortening of B-O bonds resulting from the bonding of the

oxygen with modifier cations instead of another B atom in such highly modified compositions [15]. It may be noted that this estimated fraction of BO_4 is possibly an upper limit as this spectrum was collected with a spin-echo sequence, which likely have resulted in a semi-quantitative ^{11}B NMR spectrum, due to the difference in the quadrupolar coupling constants C_Q and thus, in the nutation frequencies of the BO_3 and BO_4 units. Most likely the intensity of the BO_4 resonance is somewhat enhanced in this spectrum (Fig. 2), as this environment has a lower C_Q and thus a lower nutation frequency, compared to those for the BO_3 units. Nevertheless, it is clear that the large increase in sensitivity at such high magnetic field is crucial in enabling the detection of such small amounts of BO_4 units in this glass. Despite its small relative fraction, the presence of BO_4 units in this glass establishes beyond doubt that the oxygen speciation reaction in Eq. 1 is indeed in play and $K < \infty$. Such oxygen speciation behavior is consistent with the high cooling rate of these containerless levitation melted glasses, resulting in high T_f, which leads to an entropically favored conversion of NBO to FO + BO [5].

Previous studies in the literature have indicated that B-containing oxide glasses and liquids including borates and borosilicates display the well-known B speciation reaction [21-24]:

$$BO_4 \rightleftharpoons BO_3 + NBO \qquad (3)$$

The equilibrium of this reaction shifts to the right, being entropically favored, with increasing temperature. We have investigated the temperature dependence of this speciation reaction in the $(La_2O_3)_x (B_2O_3)_{100-x}$ glass with $x = 25$. The ^{11}B MAS NMR spectrum of the water-quenched glass with higher T_f is compared in Fig. 4 with that of the furnace-cooled glass with lower T_f. As expected, the BO_4:BO_3 ratio decreases from ~ 1:1 to 1:1.2 with increasing T_f . Although the precise cooling rates of the water-quenched and furnace-cooled glasses are not known, the

difference between the two rates is expected to be modest. However, the relatively large change in the BO_4 fraction (Fig. 4) indicates a significant difference in the T_f between the two glasses, which in turn suggests a relatively high fragility index *m* for this composition (see below).

Lastly, we note in Fig. 4 that the quadrupolar line shape of the BO_3 resonance also changes with changing T_f indicating the presence of multiple BO_3 species in these glasses and a change in their relative ratios with temperature. This inference is consistent with the simulation of the BO_3 resonance in the ^{11}B MAS NMR spectra of $(La_2O_3)_x$ $(B_2O_3)_{100-x}$ glasses of comparable compositions ($20 \leq x \leq 30$) in a previous study by Masuno et al. [16] with two distinct BO_3 sites. These authors simulated the BO_3 line shape in the ^{11}B MAS NMR spectra of these glasses with two components, which correspond to BO_3 units with different number of NBOs. The component with higher isotropic chemical shift δ_{iso} was assigned to BO_3 units with higher number of NBOs compared to the one with lower δ_{iso} [16]. We have not attempted such simulations in the present study in the absence of spectra at multiple magnetic fields or of two-dimensional ^{11}B multiple-quantum MAS data. However, a close inspection of Fig. 4 clearly shows an enhancement in the intensity of the BO_3 line shape in the region with higher δ_{iso} in the ^{11}B MAS NMR spectrum of the glass with higher T_f, which is indicative of an increase in the relative fraction of NBOs in this glass. Therefore, when taken together, both the T_f -dependence of the BO_3:BO_4 ratio and the BO_3 line shape in this glass indicate a shift of the B speciation reaction equilibrium to the right with increasing temperature.

3.2. ^{17}O NMR

The ultra-high field (35.2 T) ^{17}O MAS NMR spectrum of the $(La_2O_3)_x$ $(B_2O_3)_{100-x}$ glass with x = 25 and high field (18.8 T) ^{17}O MAS NMR spectrum of glasses with x = 55 and 60 are

shown in Fig. 5. It is clear from Fig. 5 that the ^{17}O signal from glasses with high La_2O_3 content (x = 55, 60) is much weaker compared that from the glass with a relatively low La_2O_3 content (x = 25), as B_2O_3 is the source of ^{17}O in these glasses. Besides, a general loss in ^{17}O during levitation melting in oxygen (~ 99.8% ^{16}O) due to isotopic exchange could also be substantially higher in La-rich compositions. The ^{17}O MAS NMR spectrum of the furnace-cooled glass with x = 25 (Fig. 5a) displays two resonances centered at ~ 90 and 200 ppm, which, based on the ^{17}O NMR chemical shift systematics in borates established in previous studies in the literature, can be assigned, respectively, to BO and NBO environments [18]. This ^{17}O MAS NMR spectral line shape can be simulated well with two Gaussian center bands and associated spinning sidebands corresponding to these two resonances (Fig. 5a). It may be noted that the use of Gaussian lines is appropriate here, as the quadrupolar broadening effect on the ^{17}O NMR line shape is negligible at such high magnetic fields. This simulation yields the relative fractions of NBO and BO to be ~ 24% and 76%, respectively. Therefore, out of 300 oxygen atoms in the formula unit approximately 72 are NBO, which implies a BO_4 fraction of ~ 52% in this glass. This estimate is consistent with the ^{11}B NMR result, which indicated that in this glass ~50% of the B atoms are present as BO_4 species (see above). When taken together, the ^{11}B and ^{17}O NMR results indicate that in this glass with relatively low La_2O_3 content La acts as a typical modifier cation that provides charge balance not only for the NBOs but also for any non-neutral BO atoms, e.g. those linking BO_3 and BO_4 units.

On the other hand, glasses with x = 55 and 60 are characterized by O/B > 3.0 and thus oxygen atoms are expected to be present as NBO and FO, while the relative concentration of BO environments is expected to be negligible unless $K << \infty$ in the reaction in Eq. 1. This expectation is indeed borne out in the ^{17}O MAS NMR spectra of these two glasses (Fig. 5b),

which show two resonances centered at ~ 215 and 540 ppm, while the BO resonance near 90 ppm is undetectable. As before, the resonance at ~ 215 ppm can be readily assigned to the NBO environment, which suggests that the second resonance at ~ 540 ppm corresponds to the FO environment where the oxygen atom is only bonded to La nearest neighbors. Two such FO environments are present in crystalline hexagonal La_2O_3 where the oxygen atoms are either surrounded by 5 or by 4 La nearest neighbors i.e. in $O[La]_5$ and $O[La]_4$ configurations [25]. Previous ^{17}O NMR studies have shown that these $O[La]_5$ and $O[La]_4$ environments resonate at 467 ppm and 584 ppm, respectively [26-28]. However, it is important to note that the $O[La]_5$ environment was incorrectly identified with a six-coordinated environment in these ^{17}O NMR studies. Therefore, according to this trend, the resonance at ~ 540 ppm observed in Fig. 5b may suggest the presence of an FO environment of the type $O[La]_4$ in La-borate glasses with x = 55 and 60. It may be noted that at the same time the absence of any resonance near 467 ppm negates the possibility of the crystallization of La_2O_3 in these glasses. On the other hand, the absence of any detectable signal in the region between 400 and 600 ppm in the ^{17}O spectrum of the La-borate glass with x = 25 (Fig. 5a) indicates, within the limit of detection of ~ 0.5%, the absence of any FO environment in this glass.

Further insight into the bonding of the FO with La in glasses with x = 55 and 60 can be obtained if one considers a simple bond valence type calculation for a x = 50 glass. In such a glass there are three NBO atoms per La and thus, besides one B atom, if each NBO is bonded to two La atoms then each La receives –0.5 charge from each NBO and 3 such NBO would contribute −1.5 charge. The remaining −1.5 charge would come from the FO atoms and for an $O[La]_4$ environment each FO would contribute −2/4 i.e. –0.5 charges to the La. Therefore, there can be ~ 3 such FO atoms around each La to provide the remaining −1.5 charge and thus, each La could on

an average be bonded to ~3 NBO and ~3 FO, leading to a total La-O coordination number of ~ 6.0 [29]. This rather approximate estimation of the La-O coordination number is significantly lower than the X-ray diffraction results reported in a recent study [17], which indicated an average La-O coordination number of ~ 7.7 in similar La-borate glasses. However, in the latter study, the accuracy of the estimation of this coordination number from the diffraction data was also noted to be low [17]. Integration of the areas under the resonances at ~ 215 and 540 ppm and their associated spinning sidebands in these ^{17}O NMR spectra in Fig. 5b yields ~ 9% and 13% FO, respectively, for the x = 55 and 60 glasses. These values are quite consistent with the expected FO relative fractions of 10% and 15% for these two glasses in the case of binary oxygen speciation with K = ∞ for the reaction in Eq. 1. On the other hand, the signal : noise ratio of these spectra puts a limit of detectability of BO in these glasses at ~ 3%, which yields a minimum value for K of ~ 200-300. Thus, when taken together, these ^{11}B and ^{17}O NMR results suggest that the structure of these high-La glasses with x = 55 and 60 consist of a network of LaO_6 polyhedra linked via La-O-La and La-O-B bonds with the latter via interspersed $[BO_3]^{3-}$ units.

3.3. Fragility and Configurational Entropy

The compositional variation in the T_g and the calorimetric fragility index m of $(La_2O_3)_x(B_2O_3)_{100-x}$ glasses is shown in Fig. 6. The T_g values are consistent with those reported in previous studies on $(La_2O_3)_x(B_2O_3)_{100-x}$ glasses of comparable compositions (Fig. 6a) [17,30]. The limited dataset indicates a sudden rise in T_g in glasses with $x \geq 55$, which is likely related to the appearance of a strongly bonded La-O polyhedral network in glasses with O/B >3. On the other hand, m displays a rapid increase from ~ 35 for pure B_2O_3 to ~ 90 upon the addition of up to ~ 25 mol% La_2O_3 with O/B = 2 (Fig. 6b). The temperature dependence of the viscosity data

for the $(La_2O_3)_{25}$ $(B_2O_3)_{75}$ liquid is shown in Fig. 7. These viscosity data are fitted to the standard Mauro-Yue-Ellison-Gupta-Allan (MYEGA) equation (Eqn. 4) to obtain the kinetic fragility index m_k [31]. The MYEGA equation can be written as:

$$\log \eta = \log \eta_\infty + (12 - \log \eta_\infty) \cdot \frac{T_g}{T} \cdot \exp\left[\left(\frac{m_k}{12 - \log \eta_\infty} - 1\right) \cdot \left(\frac{T_g}{T} - 1\right)\right] \qquad (4)$$

where $\log \eta_\infty$ and m_k are adjustable fitting parameters. The MYEGA fit yields a fragility index m_k ~ 94, consistent with the calorimetrically determined value of m ~ 90. Further addition of La_2O_3 to 30 mol% (O/B = 2.14) results in a slight decrease in m to ~ 84, consistent with the compositional variation of m in Li-borates reported by Matsuda et al. [32] where the TMDSC measurements indicated a maximum in m near O/B = 2, where m ~ 80, which decreases to ~70 near O/B = 2.14. In contrast to this decreasing trend, the m of a $(La_2O_3)_x (B_2O_3)_{100-x}$ glass with x = 55 corresponding to O/B = 3.33 is found to increase again to ~ 120. This rather large value of m to the best of our knowledge is the highest reported for any oxide glass-forming liquid and is the first report of the fragility index for a liquid consisting of completely isolated BO_3 triangles with ~90% of the oxygen atoms being present as NBOs and the rest as FO bonded only to La atoms.

The compositional variation of m for $(La_2O_3)_x (B_2O_3)_{100-x}$ liquids with $x \leq 30$ as discussed above is consistent with recent calculations of the temperature dependence of configurational entropy of binary alkali borate liquids by Alderman and coworkers [33]. These calculations, based on the borate speciation reaction in Eq. 3 as the dominant source of the temperature dependence of configurational entropy, indicate that m increases on addition of modifier oxide to B_2O_3 and goes through a maximum at O/B =2. The ^{11}B NMR spectra of the $(La_2O_3)_{25} (B_2O_3)_{75}$ glass with O/B = 2 indeed show quite strong temperature dependence of the borate speciation in agreement with the fragility maximum observed near this composition. Beyond this point there

are scant experimental data but Alderman et al.'s calculations [33] suggest that further addition of alkali oxide results in *m* steadily decreasing as O/B approaches ~ 3. Previous studies [16,17] indicated that $(La_2O_3)_x(B_2O_3)_{100-x}$ compositions with 2.3 < O/B < 3.0 did not form glasses. However, the present data indicate that *m* of $(La_2O_3)_x(B_2O_3)_{100-x}$ liquids probably goes through a local minimum in this composition range and increases again and becomes rather large as O/B exceeds 3, where the fragility is predominantly controlled by sources of configurational entropy other than the borate speciation reaction as the structure ceases to form a borate network at such high levels of modifier content. It is clear from the ^{11}B and ^{17}O NMR results that the structure of these glasses with O/B ≥ 3 consists of $[BO_3]^{3-}$ units which, in the absence of B-O-B linkages, may now have additional degrees of configurational freedom. In addition, the presence of ~ 0.5% BO_4 units in the glass with x = 55 suggests that the temperature dependence of structural speciation via both reactions in Eqs. 1 and 3 may contribute to configurational entropy. Therefore, when taken together, these sources of configurational entropy may be consistent with the rather large *m* observed for the liquid with x = 55.

4. Conclusions

When taken together, the ^{11}B and ^{17}O MAS NMR spectra of $(La_2O_3)_x(B_2O_3)_{100-x}$ glasses indicate that the addition of La_2O_3 to B_2O_3 in the composition range $22 \leq x \leq 30$ results in the usual conversion of BO_3 to BO_4 units in the borate network as well as the formation of NBOs to an extent, which is comparable to those reported for binary alkali borates with similar O/B ratio. Therefore, La_2O_3 acts as a typical modifier in La-borate glasses in this composition range. On the other hand, the borate network consisting of corner-sharing BO_3 and BO_4 units disappears as the La_2O_3 content becomes higher than 50 mol% in these glasses, and almost all B atoms exist as

isolated $[BO_3]^{3-}$ units. At this point the structure consists of approximately six-coordinated La-O polyhedra that share corners via approximately four-coordinated FO atoms as well as via La-O-B linkages with intervening $[BO_3]^{3-}$ units. This compositional evolution of the structure from a B-O based network to an La-O based network across $x \sim 50$ is characterized by a sharp rise in T_g by nearly 100 °C. The boron and oxygen speciation reactions $BO_4 \rightleftharpoons BO_3$+NBO and 2NBO $\rightleftharpoons$ FO + BO shift to the right with increasing T_f and contribute to increasing configurational entropy. This temperature dependence of the configurational entropy is manifested in the relatively high values of m observed in these supercooled liquids.

ACKNOWLEDGEMENT

This work is supported by the National Science Foundation Grant NSF DMR 1855176 to SS. The National High Magnetic Field Laboratory is supported by the National Science Foundation through NSF/DMR-1644779 and the State of Florida. The Development of the 36 T Series-Connected Hybrid magnet and NMR instrumentation was supported by NSF (DMR-1039938 and DMR-0603042) and NIH GM122698.

References:

[1] G. Greaves, S. Sen, Inorganic glasses, glass-forming liquids and amorphizing solids, Adv. Phys., 56 (2007) 1-166. https://doi.org/10.1080/00018730601147426.
[2] A.K. Varshneya, J.C. Mauro, Fundamentals of inorganic glasses, third ed., Elsevier, New York, 2019.
[3] J.F. Stebbins, Anionic speciation in sodium and potassium silicate glasses near the metasilicate ([Na, K] 2SiO3) composition: 29Si, 17O, and 23Na MAS NMR, J. Non Cryst. Solids-X, 6 (2020) 100049. https://doi.org/10.1016/j.nocx.2020.100049.
[4] J.F. Stebbins, J. Wu, L.M. Thompson, Interactions between network cation coordination and non-bridging oxygen abundance in oxide glasses and melts: Insights from NMR spectroscopy, Chem. Geol., 346 (2013) 34-46. https://doi.org/10.1016/j.chemgeo.2012.09.021.
[5] J.F. Stebbins, "Free" oxide ions in silicate melts: thermodynamic considerations and probable effects of temperature, Chem. Geol., 461 (2017) 2-12. https://doi.org/10.1016/j.chemgeo.2016.06.029.
[6] B. Mysen, P. Richet, Silicate glasses and melts: structure and properties, Elsevier, Amsterdam, 2005, pp 544.
[7] P.C. Hess, Physics of magmatic processes, in: R.B. Hargraves (Ed.), Princeton Univ. Press, Princeton, New Jersey, 1980, pp. 3-48.
[8] P.C. Hess, Structure, dynamics, and properties of silicate melts, in: J.F. Stebbins, P.F. McMillan, D.B. Dingwell (Eds.), Mineralogical Society of America, Washington, D.C., 1995, pp. 145-189.
[9] K.N. Dalby, H.W. Nesbitt, V.P. Zakaznova-Herzog, P.L. King, Resolution of bridging oxygen signals from O 1s spectra of silicate glasses using XPS: Implications for O and Si speciation, Geochim. Cosmochim. Acta, 71 (2007) 4297-4313. https://doi.org/10.1016/j.gca.2007.07.005.
[10] G. Adam, J.H. Gibbs, On the temperature dependence of cooperative relaxation properties in glass-forming liquids, J. Chem. Phys., 43 (1965) 139-146. https://doi.org/10.1063/1.1696442.
[11] C. Angell, Relaxation in liquids, polymers and plastic crystals—strong/fragile patterns and problems, J. Non-Cryst. Solids, 131 (1991) 13-31. https://doi.org/10.1016/0022-3093(91)90266-9.
[12] A. Winterstein-Beckmann, D. Möncke, D. Palles, E.I. Kamitsos, L. Wondraczek, Structure and properties of orthoborate glasses in the Eu2O3–(Sr, Eu) O–B2O3 quaternary, J. Phys. Chem. B, 119 (2015) 3259-3272. https://doi.org/10.1021/jp5120465.
[13] B. Topper, N.S. Tagiara, A. Herrmann, E.I. Kamitsos, D. Möncke, Yttrium and rare-earth modified lithium orthoborates: Glass formation and vibrational activity, J. Non-Cryst. Solids, 575 (2022) 121152. https://doi.org/10.1016/j.jnoncrysol.2021.121152.
[14] A. Winterstein-Beckmann, D. Möncke, D. Palles, E. Kamitsos, L. Wondraczek, Structure–property correlations in highly modified Sr, Mn-borate glasses, J. Non-Cryst. Solids, 376 (2013) 165-174. https://doi.org/10.1016/j.jnoncrysol.2013.05.029.
[15] K.I. Chatzipanagis, N.S. Tagiara, E.I. Kamitsos, N. Barrow, I. Slagle, R. Wilson, T. Greiner, M. Jesuit, N. Leonard, A. Phillips, Structure of lead borate glasses by Raman, 11B MAS, and 207Pb NMR spectroscopies, J. Non-Cryst. Solids, 589 (2022) 121660. https://doi.org/10.1016/j.jnoncrysol.2022.121660.

[16] A. Masuno, T. Iwata, Y. Yanaba, S. Sasaki, H. Inoue, Y. Watanabe, High refractive index La-rich lanthanum borate glasses composed of isolated BO3 units, Dalton Trans., 48 (2019) 10804-10811. https://doi.org/10.1039/C9DT01715A.
[17] S. Sasaki, A. Masuno, K. Ohara, Y. Yanaba, H. Inoue, Y. Watanabe, S. Kohara, Structural Origin of Additional Infrared Transparency and Enhanced Glass-Forming Ability in Rare-Earth-Rich Borate Glasses without B–O Networks, Inorg. Chem., 59 (2020) 13942-13951. https://doi.org/10.1021/acs.inorgchem.0c01567.
[18] J.F. Stebbins, P. Zhao, S. Kroeker, Non-bridging oxygens in borate glasses: characterization by 11B and 17O MAS and 3QMAS NMR, Solid State Nucl. Magn. Reson., 16 (2000) 9-19. https://doi.org/10.1016/S0926-2040(00)00050-3.
[19] S. Wei, G.J. Coleman, P. Lucas, C.A. Angell, Glass transitions, semiconductor-metal transitions, and fragilities in Ge− V− Te (V= As, Sb) liquid alloys: The difference one element can make, Phys. Rev. Appl., 7 (2017) 034035. https://doi.org/10.1103/PhysRevApplied.7.034035.
[20] A.C. Wright, Borate structures: crystalline and vitreous, Chem. Glasses: Eur. J. Glass Sci. Technol. B, 51 (2010) 1-39.
[21] J.F. Stebbins, S.E. Ellsworth, Temperature effects on structure and dynamics in borate and borosilicate liquids: high-resolution and high-temperature NMR results, J. Am. Ceram. Soc., 79 (1996) 2247-2256. https://doi.org/10.1111/j.1151-2916.1996.tb08969.x.
[22] L. Cormier, O. Majérus, D. Neuville, G. Calas, Temperature-Induced Structural Modifications Between Alkali Borate Glasses and Melts, J. Am. Ceram. Soc., 89 (2006) 13-19. https://doi.org/10.1111/j.1551-2916.2005.00657.x.
[23] O.L. Alderman, C.J. Benmore, A. Lin, A. Tamalonis, J.R. Weber, Borate melt structure: Temperature-dependent B–O bond lengths and coordination numbers from high-energy X-ray diffraction, J. Am. Ceram. Soc., 101 (2018) 3357-3371. https://doi.org/10.1111/jace.15529.
[24] S. Sen, Temperature induced structural changes and transport mechanisms in borate, borosilicate and boroaluminate liquids: high-resolution and high-temperature NMR results, J. Non-Cryst. Solids, 253 (1999) 84-94. https://doi.org/10.1016/S0022-3093(99)00346-4.
[25] G.-y.A. Gy, N. Imanaka, The binary rare earth oxides, Chem. Rev., 98 (1998) 1479-1514. https://doi.org/10.1021/cr940055h.
[26] F. Ali, M.E. Smith, S. Steuernagel, H.J. Whitfield, 17 O Solid-state NMR examination of La2O3 formation, J. Mat. Chem., 6 (1996) 261-264. https://doi.org/10.1039/JM9960600261.
[27] T. Bastow, S. Stuart, 17O NMR in simple oxides, Chem. Phys., 143 (1990) 459-467. https://doi.org/10.1016/0301-0104(90)87025-7.
[28] S. Yang, J. Shore, E. Oldfield, Oxygen-17 Nuclear magnetic resonance spectroscopic study of the lanthanide oxides, J. Magn. Reson, 99 (1992) 408-412. https://doi.org/10.1016/0022-2364(92)90195-D.
[29] J. Lin, M. Su, K. Wurst, E. Schweda, The structure of La26 (BO3) 8O27: a structure with a distorted fluorite type arrangement of atoms, J. Solid State Chem., 126 (1996) 287-291. https://doi.org/10.1006/jssc.1996.0339.
[30] I.N. Chakraborty, J.E. Shelby, R.A. Condrate, Properties and structure of lanthanum borate glasses, J. Am. Ceram. Soc., 67 (1984) 782-785. https://doi.org/10.1111/j.1151-2916.1984.tb19700.x.
[31] J.C. Mauro, Y. Yue, A.J. Ellison, P.K. Gupta, D.C. Allan, Viscosity of glass-forming liquids, Proc. Natl. Acad. Sci., 106 (2009) 19780-19784. https://doi.org/10.1073/pnas.0911705106.

[32] Y. Matsuda, Y. Fukawa, M. Kawashima, S. Mamiya, S. Kojima, Dynamic glass transition and fragility of lithium borate binary glass, Solid State Ion., 179 (2008) 2424-2427. https://doi.org/10.1016/j.ssi.2008.09.011.
[33] O.L. Alderman, C.J. Benmore, B. Reynolds, B. Royle, S. Feller, J. Weber, Liquid fragility maximum in lithium borate glass-forming melts related to the local structure, Int J Appl Glass Sci., (2022). https://doi.org/10.1111/ijag.16611.
[34] G.D. Chryssikos, J. Duffy, J. Hutchinson, M. Ingram, E. Kamitsos, A. Pappin, Lithium borate glasses: a quantitative study of strength and fragility, J. Non-Cryst. Solids, 172 (1994) 378-383. https://doi.org/10.1016/0022-3093(94)90460-X.

Figure 1

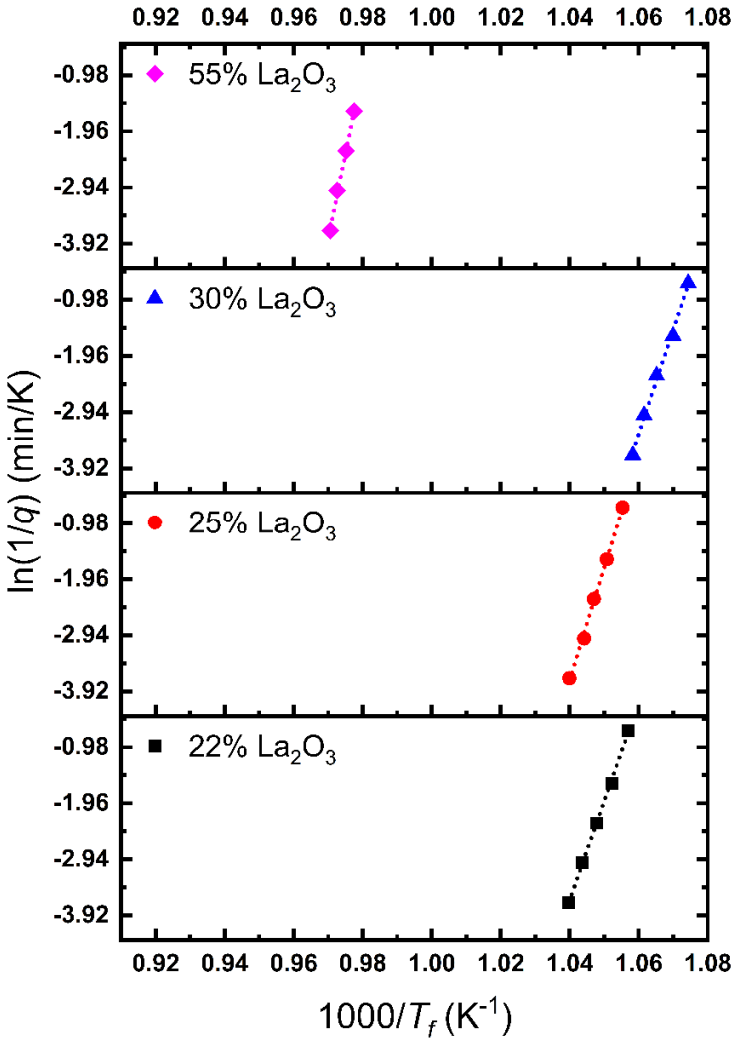

Fig. 1. Heating rate q vs. fictive temperature T_f of $(La_2O_3)_x(B_2O_3)_{100-x}$ glasses.

Figure 2

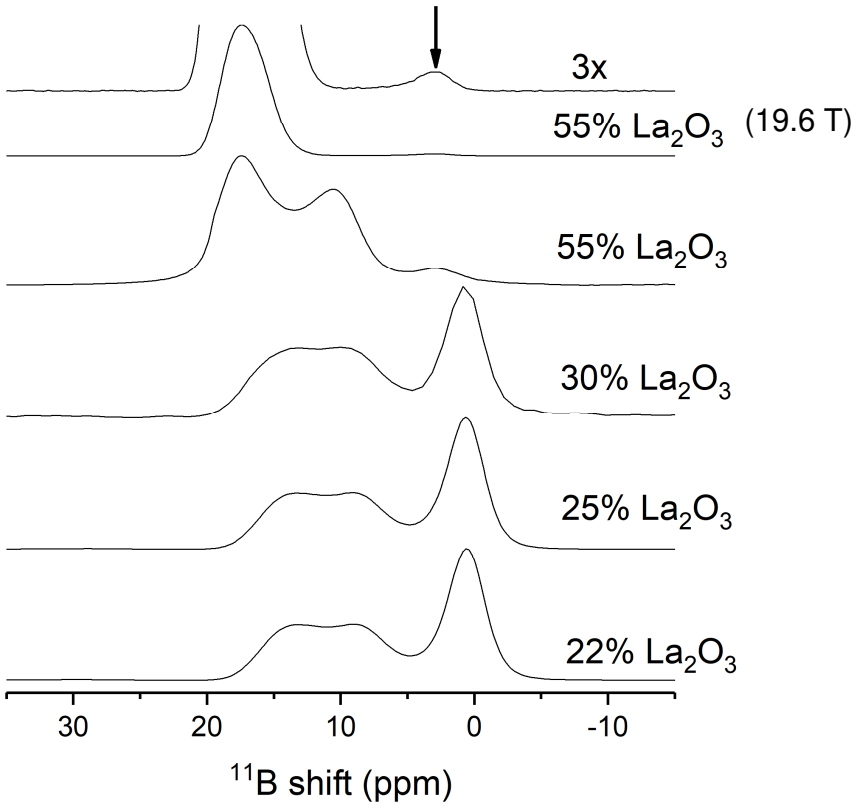

Fig. 2. ^{11}B MAS spectra of $(La_2O_3)_x(B_2O_3)_{100-x}$ glasses. Compositions are shown alongside the spectra. All spectra were taken at 11.7 T, except for the second spectrum from top, which was taken at 19.6 T. A 3x magnified view of this spectrum is shown at the very top with arrow indicating BO_4 resonance.

Figure 3

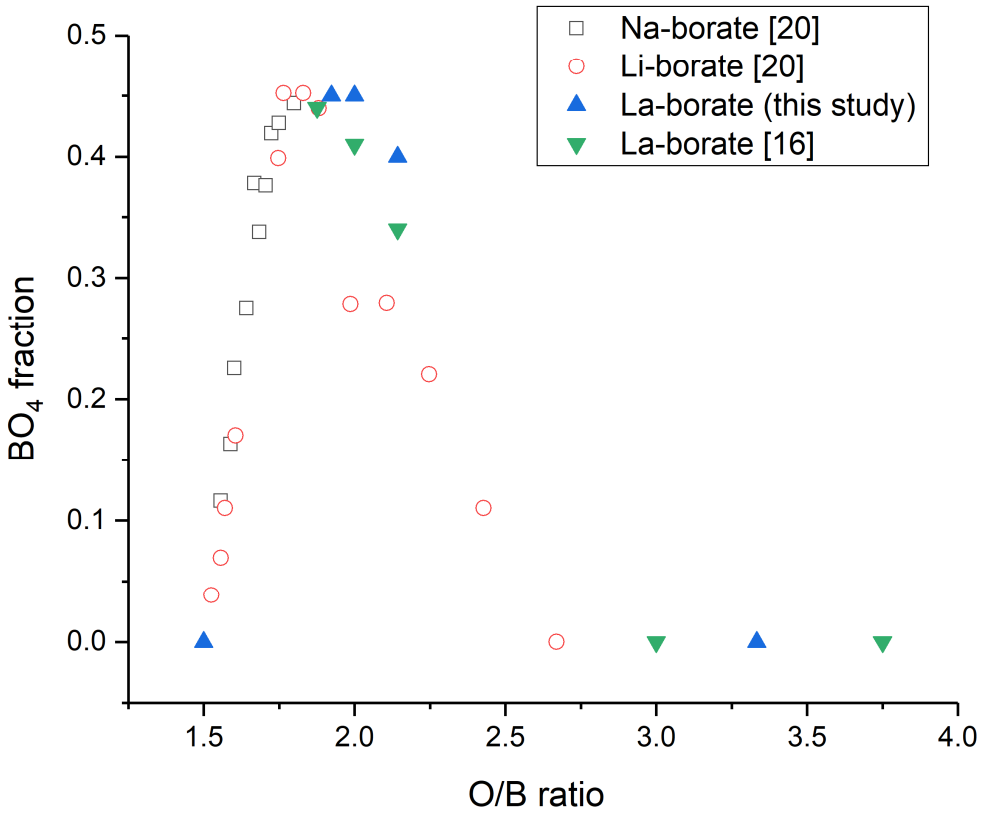

Fig. 3. Fraction of B present as BO_4 units in alkali borate (open squares and circles) and La-borate glasses (solid triangles) as a function of O/B ratio. Alkali borate data are from a literature compilation by Wright [20]. La-borate data from present study are shown as upright triangles and those from a previous study [16] are shown as inverted triangles.

Figure 4

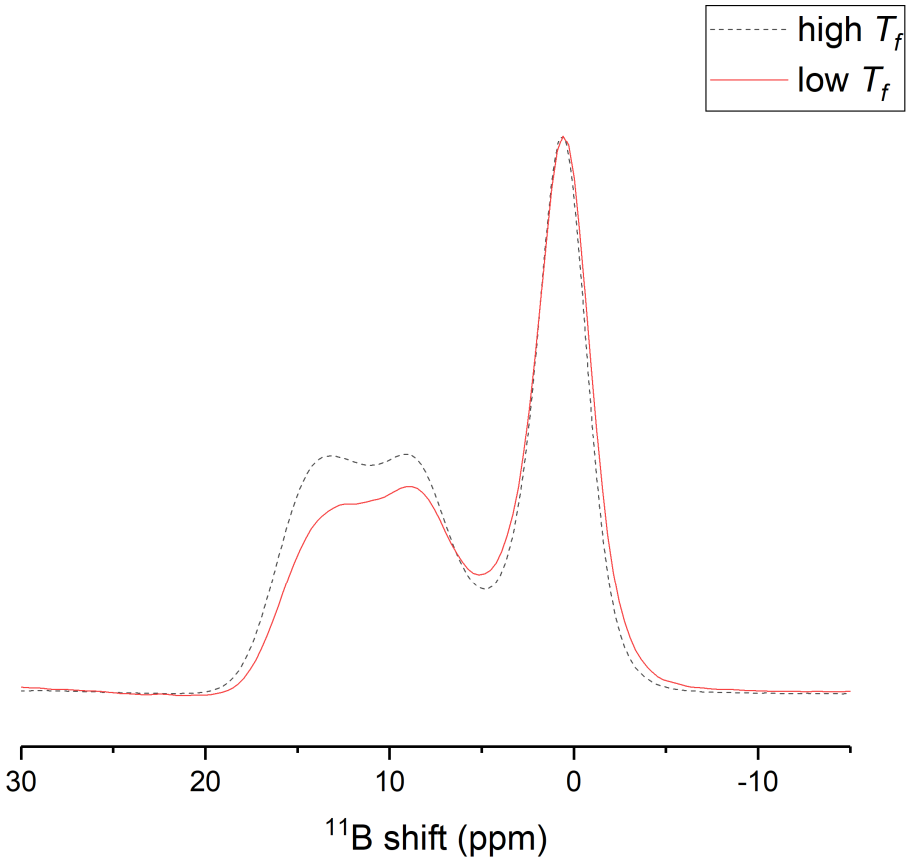

Fig. 4. ^{11}B MAS spectra of $(La_2O_3)_{25}(B_2O_3)_{75}$ glasses with high (dashed line) and low (solid line) T_f.

Figure 5a

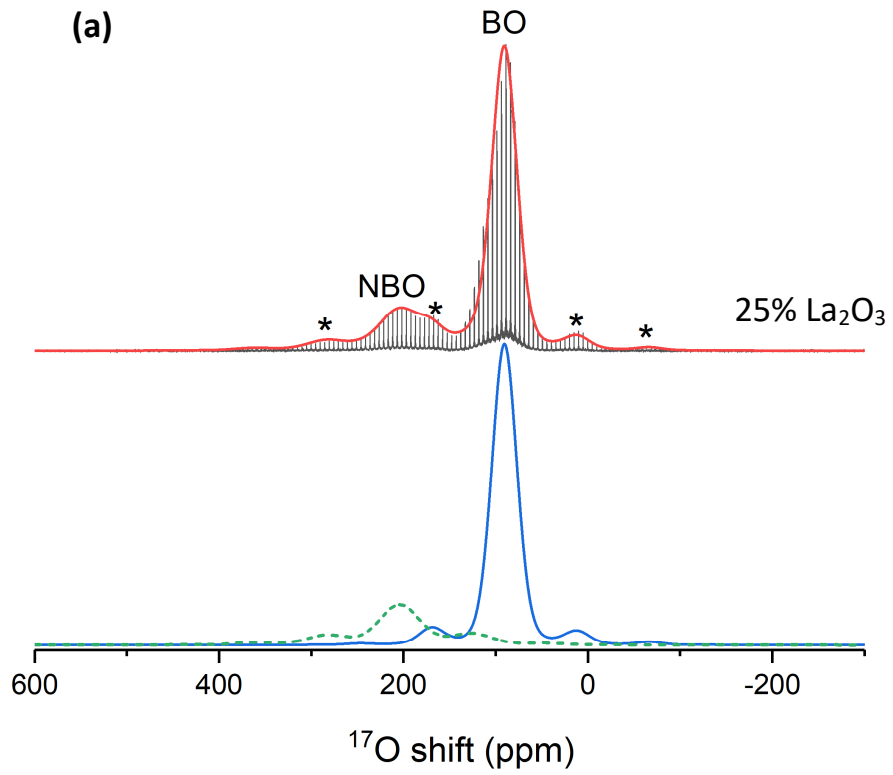

Fig. 5a. Top: Experimental (spikelet pattern) and simulated (solid red line) ultra-high field (35.2 T) ^{17}O (WURST-QCPMG) MAS spectrum of $(La_2O_3)_{25}(B_2O_3)_{75}$ glass. Asterisks denote spinning sidebands. Resonances corresponding to BO and NBO sites are marked on the spectra. Bottom: The center band and spinning sidebands of individual simulation components for BO and NBO environments are shown, respectively, with solid and dashed lines with a vertical offset for clarity.

Figure 5b

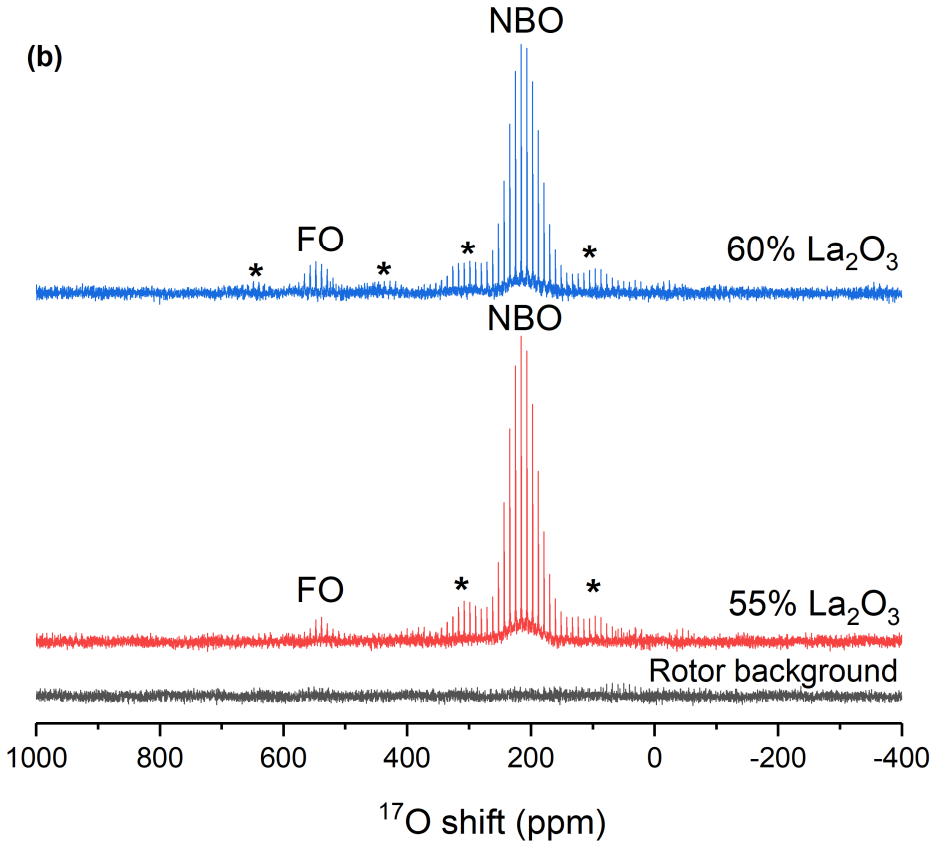

Fig. 5b. ^{17}O (WURST-QCPMG) MAS spectrum of invert $(La_2O_3)_x(B_2O_3)_{100-x}$ glasses with x = 60 (top), x=55 (middle) and of background signal from empty rotor (bottom) collected at 18.8 T. Asterisks denote spinning sidebands. Resonances corresponding to FO and NBO sites are marked on the spectra.

Figure 6a

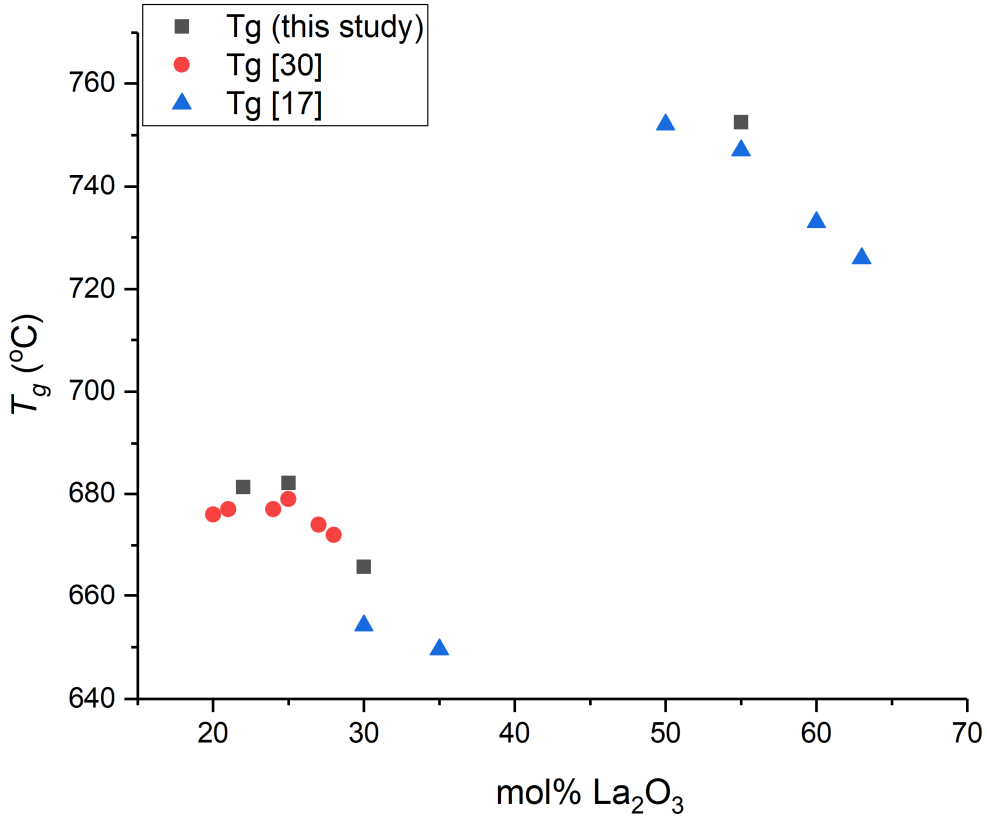

Fig. 6a. Compositional variation in T_g of $(La_2O_3)_x(B_2O_3)_{100-x}$ glasses determined in this study (squares) and reported in previous studies (circles and triangles) [17,30].

Figure 6b

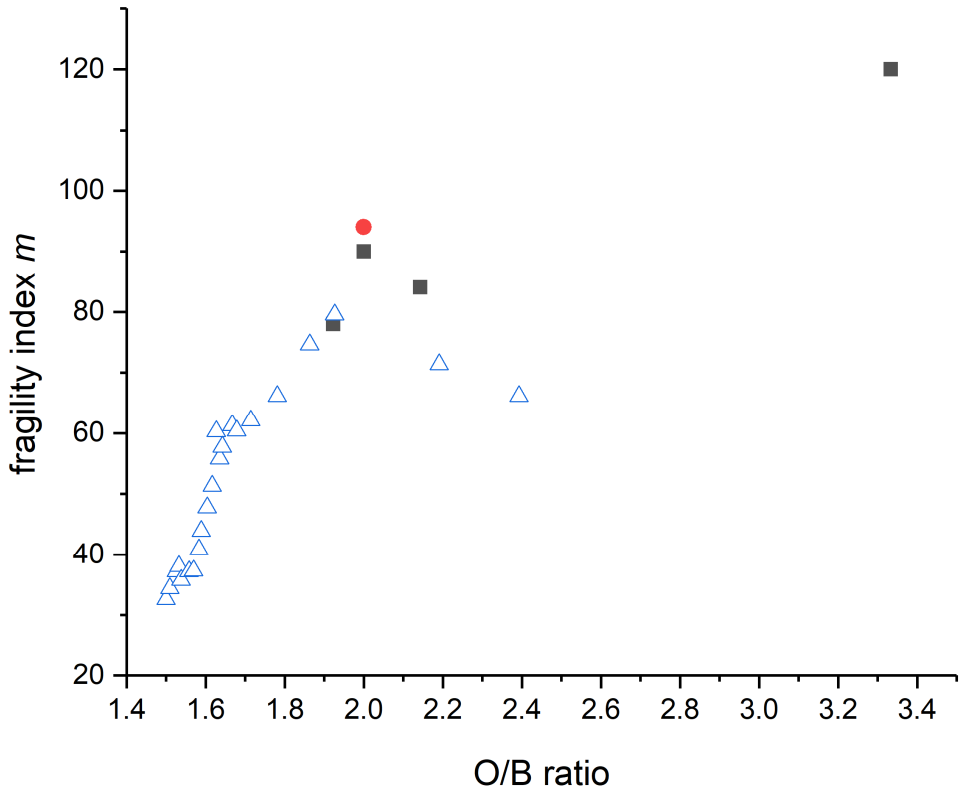

Fig. 6b. Compositional variation in fragility index *m* of $(La_2O_3)_x(B_2O_3)_{100-x}$ glasses determined in this study using calorimetry (filled squares) and those reported in previous studies for $(Li_2O)_x(B_2O_3)_{100-x}$ glasses (open triangles) [32-34]. Red filled circle corresponds to *m* determined from viscosity for $(La_2O_3)_{25}(B_2O_3)_{75}$ composition (see text for details).

Figure 7

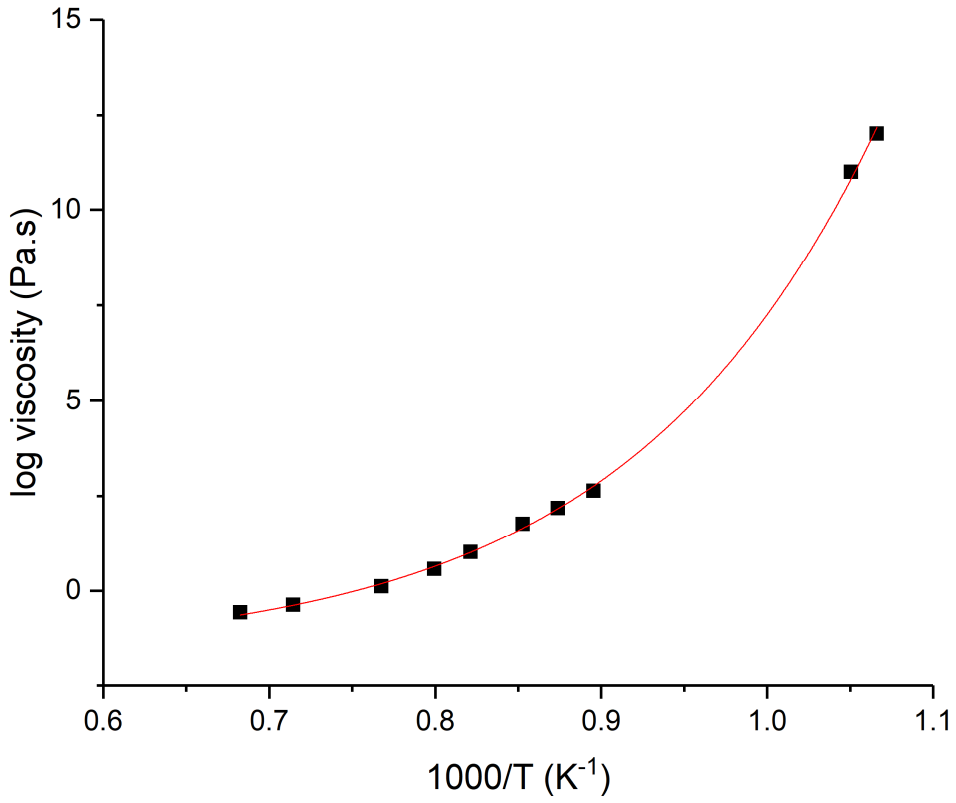

Fig. 7. Temperature dependence of viscosity of $(La_2O_3)_{25}(B_2O_3)_{75}$ liquid. Solid line through datapoints is a fit of MYEGA equation to experimental data. All viscosity values below 10^5 Pa.s are measured in the present study. Calorimetric T_g obtained at a heating rate of 10K/min is taken to be the temperature corresponding to a viscosity of 10^{12} Pa.s, while the datapoint at 10^{11} Pa.s is taken from a previous study [30].